Available online at www.sciencedirect.com
SCIENCE DIRECT®
Chemical Physics Letters 392 (2004) 383–389
CHEMICAL PHYSICS LETTERS
www.elsevier.com/locate/cplett

Electron–phonon interaction and relaxation time in graphite

J. Jiang [a,*], R. Saito [a], A. Grüneis [a], G. Dresselhaus [b], M.S. Dresselhaus [c,d]

[a] Department of Physics, Tohoku University and CREST, JST, Aramaki, Aoba, Sendai 980-8578, Japan
[b] Francis Bitter Magnet Laboratory, Massachusetts Institute of Technology, Cambridge, MA 02139-4307, USA
[c] Department of Physics, Massachusetts Institute of Technology, Cambridge, MA 02139-4307, USA
[d] Department of Electrical Engineering and Computer Science, Massachusetts Institute of Technology, Cambridge, MA 02139-4307, USA

Received 6 March 2004
Available online 15 June 2004

Abstract

The electron–phonon (e–ph) interaction and the relaxation time of photo-excited electrons are calculated in graphite within the tight-binding scheme. The e–ph matrix element thus obtained, shows anisotropy in k-space. The calculated relaxation time is of the same order of magnitude as the experimental one. Moreover, below an energy close to the Fermi energy, the absorption rate exceeds the emission rate, which indicates that graphite can emit far infra-red electro-magnetic waves by absorbing heat. We also compare this result with Planck's formula for black-body radiation.

1. Introduction

Advances in ultrafast laser technology allow us to investigate the ultrafast dynamics of electron excitations in solids and to further our understanding of the fundamental scattering processes in solids at the femtosecond time scale [1,2]. By using ultrafast laser technology, the electron–phonon (e–ph) coupling strength and the photo-excited electron relaxation time in carbon nanotubes and graphite have been the subject of continuing studies [3–7]. The strength of the e–ph interaction plays a key role in a variety of physical phenomena, such as the temperature dependence of the electrical conductivity and possible superconductivity [8,9].

The e–ph scattering process in single wall carbon nanotubes and graphite is relevant to recent hot topics such as photoluminescence, Raman spectra, and transport [10–17]. Graphite is a material which does not emit light because there is no energy gap between the conduction and valence energy bands. On the other hand, carbon strongly emits far infra-red electro-magnetic waves. In graphite the dynamics of photo-excited carriers are dominated by both electron–electron (e–e) and e–ph scattering. After optical excitation, the electrons are thermalized by e–e scattering on a time scale shorter than 50 fs [3,6]. The electron and hole distributions then relax to their respective band extrema by e–ph scattering in about 1 ps [3]. For the e–e scattering process (referred to as internal thermalization), femtosecond time-resolved photo-emission of photo-excited electrons in highly oriented pyrolytic graphite provides strong evidence for anisotropies in the quasi-particle lifetimes and thus the energy dependence of the e–e decay rates cannot be described by a $(E - E_F)^2$ dependence, as would be expected by Fermi liquid theory [18]. By considering that femtosecond time-resolved experiments can now reveal the whole photo-excited electron relaxation process, it is very interesting to study the electron relaxation times for the whole e–ph scattering process in graphite [3]. In this Letter, we focus our attention on the e–ph interaction. We calculate the e–ph interaction up to 4th nearest-neighbor sites within the tight-binding framework. We find that among the six phonon modes, the four in-plane modes contribute to the e–ph. The obtained e–ph matrix elements around the K point for the Γ point phonon modes show strong anisotropy. Moreover, we calculate the relaxation time

* Corresponding author. Fax: +0222176475.
E-mail address: jiang@flex.phys.tohoku.ac.jp (J. Jiang).

0009-2614/$ - see front matter © 2004 Elsevier B.V. All rights reserved.
doi:10.1016/j.cplett.2004.05.097

of photo-excited electrons over a wide energy region. We find that because of the peculiar structure of the Fermi surface of graphite, the dominant processes for the relaxation rates reverse near the Fermi level, at which point far infra-red photon emission is expected.

2. Electron–phonon matrix element and relaxation time

A periodic displacement of the atomic potential around the equilibrium sites of a system gives rise to the e–ph interaction which can be treated in first-order time-dependent perturbation theory. We can write an interaction Hamiltonian for the e–ph system in the form

$$H^{\nu}_{\mathrm{e-ph}} = \langle \Psi(\mathbf{r},\mathbf{k}',t)|\delta V^{\nu}(\mathbf{r},\mathbf{q},t)|\Psi(\mathbf{r},\mathbf{k},t)\rangle, \tag{1}$$

where $\Psi(\mathbf{r},\mathbf{k}',t)$ and $\Psi(\mathbf{r},\mathbf{k},t)$ are the initial and final electron states, and $\delta V^{\nu}(\mathbf{r},\mathbf{q},t)$ is a phonon-induced perturbed deformation potential denoted by the phonon branch with index ν. Here we focus on the e–ph interaction for electrons in the conduction band. The wave function $\Psi(\mathbf{r},\mathbf{k},t)$ for conduction band electron states in graphite is given by

$$\Psi_l(\mathbf{r},\mathbf{k},t) = \frac{1}{\sqrt{N_{\mathrm{u}}}}\sum_{l=1}^{N_{\mathrm{u}}}\sum_{s=A,B} C_s(\mathbf{k})\mathrm{e}^{\mathrm{i}[\mathbf{k}\cdot(\mathbf{R}_l+\mathbf{r}_l)-\omega(\mathbf{k})t]} \times \phi(\mathbf{r}-\mathbf{R}_l-\mathbf{r}_s), \tag{2}$$

where $\omega(\mathbf{k}) = E(\mathbf{k})/\hbar$, and $\phi(\mathbf{r}-\mathbf{R}_l-\mathbf{r}_s), (l=1,\ldots,N_{\mathrm{u}})$, is the $2p_z$ orbital of carbon, and N_{u} denotes the number of unit cells in the solid. The coefficient $C_s(\mathbf{k})$ and the energy $E(\mathbf{k})$ are obtained by solving the 2×2 Hamiltonian matrix [19],

$$C_A(\mathbf{k}) = -\frac{1}{\sqrt{2}}, \quad C_B(\mathbf{k}) = \frac{f(\mathbf{k})^*}{\sqrt{2}w(\mathbf{k})}, \quad E(\mathbf{k}) = \gamma_0 w(\mathbf{k}), \tag{3}$$

with

$$f(\mathbf{k}) = \mathrm{e}^{\mathrm{i}k_x a/\sqrt{3}} + 2\mathrm{e}^{-\mathrm{i}k_x a/2\sqrt{3}}\cos\left(\frac{k_y a}{2}\right), \quad w(\mathbf{k}) = \sqrt{|f(\mathbf{k})|^2}, \tag{4}$$

where $\gamma_0(=2.9$ eV) is nearest neighbor transfer integral and $a(=0.246$ nm) is the lattice constant of graphite.

The deformation potential $\delta V^{\nu}(\mathbf{r},\mathbf{q},t)$, including all atoms in the graphite sample, is given by

$$\delta V^{\nu}(\mathbf{r},\mathbf{q},t) = -\sum_{i=1}^{N_{\mathrm{u}}}\sum_{\sigma=A,B}\mathbf{u}^{\nu}_{i\sigma}(\mathbf{q})\cdot\nabla v(\mathbf{r}-\mathbf{R}_i-\mathbf{r}_\sigma), \tag{5}$$

where $\mathbf{u}^{\nu}_{i\sigma}(\mathbf{q})$ is the atomic displacement and $v(\mathbf{r}-\mathbf{R}_i-\mathbf{r}_\sigma)$ is the atomic potential at the site $\mathbf{r}_\sigma$ in the unit cell $\mathbf{R}_i$. In terms of the phonon eigenvector $\mathbf{e}^{\nu}_{\sigma}(\mathbf{q})$, we get an expression for the atomic displacement,

$$\mathbf{u}^{\nu}_{i\sigma}(\mathbf{q}) = \frac{1}{2}A^{\nu}(\mathbf{q})\mathbf{e}^{\nu}_{\sigma}(\mathbf{q})\mathrm{Re}\left[\mathrm{e}^{\mathrm{i}\{\mathbf{q}\cdot(\mathbf{R}_{\mathbf{i}}+\mathbf{r}_\sigma)-\omega^{\nu}(\mathbf{q})t\}}\right], \tag{6}$$

where $A^{\nu}(\mathbf{q})$ is the atomic vibration amplitude, $\omega^{\nu}(\mathbf{q})$ is the phonon eigenvalue, and $\mathrm{Re}[\cdots]$ denotes the real part of a complex function. The phonon eigenvalues and eigenvectors can be obtained by solving the 6×6 dynamical matrix [19]. The atomic vibration amplitude $A^{\nu}(\mathbf{q})$ is expressed by the phonon number $n^{\nu}(\mathbf{q})$,

$$A^{\nu}(\mathbf{q}) = \left[\frac{\hbar}{N_{\mathrm{u}}M\omega^{\nu}(\mathbf{q})}n^{\nu}(\mathbf{q})\right]^{1/2}, \tag{7}$$

where M is the mass of carbon atom. The phonon number can be expressed by the Bose–Einstein distribution function $n^{\nu}(\mathbf{q})$. For phonon emission, $n^{\nu}(\mathbf{q})$ is given by

$$n^{\nu}(\mathbf{q}) = \frac{1}{\mathrm{e}^{\beta\hbar\omega}-1}+1, \tag{8}$$

and for phonon absorption we have:

$$n^{\nu}(\mathbf{q}) = \frac{1}{\mathrm{e}^{\beta\hbar\omega}-1}, \tag{9}$$

where $\beta = 1/k_{\mathrm{B}}T$ and k_{B} is the Boltzmann constant. Substituting Eqs. (2), (5) and (6) into Eq. (1), $H^{\nu}_{\mathrm{e-ph}}$ is expressed as

$$H^{\nu}_{\mathrm{e-ph}} = -\frac{1}{2}A^{\nu}(\mathbf{q})D^{\nu}(\mathbf{k},\mathbf{k}')\left[\mathrm{e}^{-\mathrm{i}\left(\omega(\mathbf{k})-\omega(\mathbf{k}')+\omega^{\nu}(\mathbf{q})\right)t}\delta_{\mathbf{k}'-\mathbf{k},\mathbf{q}} + \mathrm{e}^{-\mathrm{i}\left(\omega(\mathbf{k})-\omega(\mathbf{k}')-\omega^{\nu}(\mathbf{q})\right)t}\delta_{\mathbf{k}-\mathbf{k}',\mathbf{q}}\right].$$

Here, we define the e–ph matrix element $D^{\nu}(\mathbf{k},\mathbf{k}')$ that scatters an electron from $\mathbf{k}$ to $\mathbf{k}'$,

$$D^{\nu}(\mathbf{k},\mathbf{k}') = -\sum_{l,l'=1}^{N_{\mathrm{u}}}\sum_{s,s',\sigma=A,B} C^*_{s'}(\mathbf{k}')C_s(\mathbf{k}) \times \mathbf{m}_\sigma(\mathbf{R}_{l'},\mathbf{r}_{s'},\mathbf{R}_l,\mathbf{r}_s)\cdot\mathbf{e}^{\nu}_{\sigma}(\mathbf{q}) \times \mathrm{e}^{-\mathrm{i}\mathbf{k}'\cdot(\mathbf{R}_{l'}+\mathbf{r}_{l'}-\mathbf{r}_{\sigma'})}\mathrm{e}^{\mathrm{i}\mathbf{k}\cdot(\mathbf{R}_l+\mathbf{r}_l-\mathbf{r}_\sigma)}, \tag{11}$$

where $\mathbf{m}_\sigma(\mathbf{R}_{l'},\mathbf{r}_{s'},\mathbf{R}_l,\mathbf{r}_s)$ is the atomic deformation potential vector,

$$\mathbf{m}_\sigma(\mathbf{R}_{l'},\mathbf{r}_{s'},\mathbf{R}_l,\mathbf{r}_s) = \int \phi^*(\mathbf{r}-\mathbf{R}_{l'}-\mathbf{r}_{s'}-\mathbf{r}_\sigma) \times\nabla v(\mathbf{r})\phi(\mathbf{r}-\mathbf{R}_l-\mathbf{r}_s-\mathbf{r}_\sigma)\mathrm{d}\mathbf{r}. \tag{12}$$

From Eq. (10), the scattering probability from an initial $\mathbf{k}$ state to a final $\mathbf{k}'$ state is given by Fermi's golden rule,

$$\begin{aligned} W^{\nu}_{\mathbf{k}\to\mathbf{k}'} &= \frac{1}{\hbar^2}\frac{1}{t'}\lim_{t'\to\infty}\left|\int_0^{t'} H^{\nu}_{\mathrm{e-ph}}\mathrm{d}t\right|^2 \\ &= \left(\frac{\pi}{2\hbar}\right)A^{\nu}(\mathbf{q})^2|D^{\nu}(\mathbf{k},\mathbf{k}')|^2 \\ &\quad\times\left[\delta\left\{E(\mathbf{k})-E(\mathbf{k}')+\hbar\omega^{\nu}(\mathbf{q})\right\}\delta_{\mathbf{k}'-\mathbf{k},\mathbf{q}} + \delta\left\{E(\mathbf{k})-E(\mathbf{k}')-\hbar\omega^{\nu}(\mathbf{q})\right\}\delta_{\mathbf{k}-\mathbf{k}',\mathbf{q}}\right]. \end{aligned} \tag{13}$$

The first and second terms in Eq. (13) correspond to the absorption and emission probabilities, respectively, and the two δ functions provide for energy and quasi-momentum conservation. The scattering probability from an initial state $\mathbf{k}$ to all possible final states $\mathbf{k}'$ is given by

$$W^{\nu}_{\mathbf{k}} = \frac{S}{4\pi M}\left[\oint_{\omega^{\nu}=\omega(\mathbf{k}')-\omega(\mathbf{k})} \frac{|D^{\nu}(\mathbf{k},\mathbf{k}')|^2}{|\nabla_{k'}E(\mathbf{k}')|}\frac{n^{\nu}(\mathbf{k}'-\mathbf{k})}{\omega^{\nu}(\mathbf{k}'-\mathbf{k})}\mathrm{d}l'_{\nu} + \oint_{\omega^{\nu}=\omega(\mathbf{k})-\omega(\mathbf{k}')} \frac{|D^{\nu}(\mathbf{k},\mathbf{k}')|^2}{|\nabla_{k'}E(\mathbf{k}')|}\frac{n^{\nu}(\mathbf{k}-\mathbf{k}')}{\omega^{\nu}(\mathbf{k}-\mathbf{k}')}\mathrm{d}l'_{\nu}\right], \tag{14}$$

where $S=\sqrt{3}a^2/2$ is the area of a 2D graphite unit cell and the integration is along a closed contour in k space that satisfies both energy and momentum conservation. From Eq. (14), it follows that

$$W^{\nu}(E) = \frac{1}{N}\sum_{\mathbf{k}} W^{\nu}_{\mathbf{k}}\delta_{E(\mathbf{k})-E}, \tag{15}$$

where N is the number of states on an equi-energy contour. Using this scattering probability, we can calculate the relaxation time,

$$\tau^{\nu}(E) = \frac{1}{W^{\nu}(E)}, \quad \text{and} \quad \tau(E) = \frac{1}{\sum_{\nu} W^{\nu}(E)}, \tag{16}$$

where $\tau^{\nu}(E)$ is the relaxation time associated with the νth phonon branch and $\tau(E)$ is the total relaxation time, including the contribution from all branches.

3. Results and discussions

We fit the carbon $2p_z$ orbital and the carbon atomic potential by a set of Gaussians to calculate $\mathbf{m}_{\sigma}$. Eq. (12) indicates that the deformation potential vector $\mathbf{m}_{\sigma}$ is a three center integral, i.e., with a potential center and two electron centers. The potential center can be on an A or B atom site and we select this center as the origin. The two electron centers are on the some of neighboring sites of the potential center. The calculated $|\mathbf{m}_{\sigma}|$ has a maximum value (≈ 6.70 eV/Å) when the two electron centers are at the same site and the potential center is on a nearest-neighbor site. The deformation potential vector $|\mathbf{m}_{\sigma}|$ has a second maximum value (≈ 3.34 eV/Å) when one electron has the same center as the potential and another electron center is on a nearest-neighbor site. For both cases, $\mathbf{m}_{\sigma}$ is a vector along the bond direction. It is worth noting that the on-site e–ph coupling has not been considered before [20,21]. Here, we find that the on-site e–ph coupling has a larger $|\mathbf{m}_{\sigma}|$ value than the off-site coupling and cannot be neglected. We note that $|\mathbf{m}_{\sigma}|$ will not have a negligible value, even if either or both of the two electron centers are beyond the nearest-neighbor site. However, the magnitude of $\mathbf{m}_{\sigma}$ quickly decreases with increasing distance, and when the electron center extends beyond 4th nearest-neighbors, $|\mathbf{m}_{\sigma}|$ is smaller than 0.2 eV/Å. Thus we consider electron centers up to 4th nearest-neighbors.

The carbon $2p_z$ orbital wave function and carbon atomic potential have the forms $\phi(\mathbf{r}-\mathbf{r}_0)=zf(|\mathbf{r}-\mathbf{r_0}|)$ and $v(\mathbf{r})=\frac{1}{r}g(|\mathbf{r}|)$. From Eq. (12), it is clear that $\mathbf{m}_{\sigma}$ does not have a z-component that would be coupled to out-of-plane phonon modes. It thus follows that the e–ph out-of-plane modes do not contribute to the e–ph coupling of graphite (see Eq. (11)). In the graphite phonon dynamical matrix, out-of-plane modes are decoupled from in-plane modes. Thus we can further reduce the 6×6 dynamical matrix to a 4×4 dynamical matrix to obtain only in-plane modes. After picking out the out-of-plane modes, the remaining four in-plane branches consist of tangential acoustic (TA), longitudinal acoustic (LA), tangential optic (TO), and longitudinal optic (LO) branches, listed in order of increasing energy around the Γ point of the Brillouin zone (BZ) [19].

There are two inequivalent corners (K and K' points) in the hexagonal BZ. For an initial electron state $\mathbf{k}$, there are two possibilities for selecting the final electron $\mathbf{k}'$ vector and the phonon $\mathbf{q}$ vector, which satisfy both energy and momentum conservation. One possibility for $\mathbf{q}$ is electron scattering within the same K (or K') point and the other is electron scattering from the K to K' point (or from the K' to K point), which we call intra-valley and inter-valley scattering, respectively [16]. These two scattering processes are observed by the double resonance Raman spectroscopy mechanism [16]. For each phonon branch, the final electron vectors are on a closed contour around the K (or K') point and a closed contour around the K' (or K) point. Correspondingly, phonon vectors exist on a closed contour around the Γ point and on a closed contour around the K' (or K) point [16].

In Fig. 1 we show two possible sets of $\mathbf{k}'$ and $\mathbf{q}$ vectors for a given $\mathbf{k}$: (a) for the two tangential branches (TA and TO) in the case of intra-valley emission scattering, and (b) for the two longitudinal branches (LA and LO) in the case of inter-valley emission scattering. From the figure, we can see that it is not easy to distinguish between the two closed contours for the TA and TO or the LA and LO branches. The reason is that the largest phonon energy difference between any two phonon branches is about 0.2 eV, which is much smaller than the electron energy dispersion over the BZ. The phonon emission and absorption processes also have different energy and momentum conservation conditions. For phonon emission, the phonon vector and frequency satisfy $\mathbf{q}=\mathbf{k}-\mathbf{k}'$ and $\omega^{\nu}(\mathbf{q})=\omega(\mathbf{k})-\omega(\mathbf{k}')$. For phonon absorption, the conditions are $\mathbf{q}=\mathbf{k}'-\mathbf{k}$ and $\omega^{\nu}(\mathbf{q})=\omega(\mathbf{k}')-\omega(\mathbf{k})$. Thus for a given initial state, the final states are similar for the two processes due to the small magnitude for the phonon energy, while the possible $\mathbf{q}$ vectors appear on opposite sides of the Γ point.

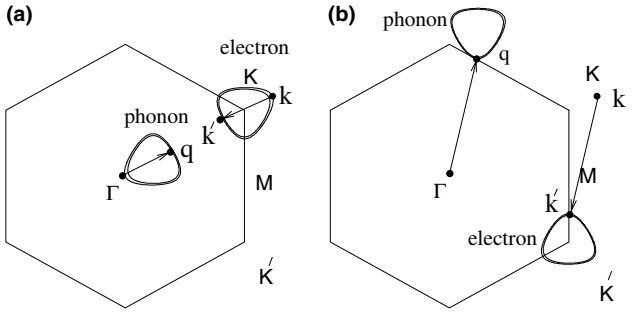

Fig. 1. For a k state (black dot) around the K point with energy $E = 2$ eV, the possible final $\mathbf{k}'$ states and phonon $\mathbf{q}$ vector (solid lines) are shown for two cases: (a) *intra-valley* phonon emission scattering. The final electron states (two contours) and phonon states (two contours) are around the K and Γ points, respectively. The outer and inner contours are results for the TA and TO branch modes, respectively. (b) *inter-valley* phonon emission scattering. The final electron states (two contours) and phonon states (two contours) are around two K' points, respectively. The outer and inner contours are results for the LA and LO branch modes, respectively.

Eq. (11) indicates that the e–ph matrix element depends on the initial and final electron states and on the phonon state. If the initial and final electron states are identical, which corresponds to the case of the first-order resonance Raman spectral process, only Γ point phonon modes contribute to the e–ph coupling. For this case, we show in Fig. 2 the $D^{\nu}(\mathbf{k},\mathbf{k})$ dependence on $\mathbf{k}$, with $\mathbf{k}$ located on an energy contour of $E(\mathbf{k}) = 1$ eV around the K point. The matrix elements for acoustic modes are zero and the matrix elements for optical modes show quite an anisotropic behavior around the K point. The anisotropy comes from the oscillation of the electron wave function coefficients $C_s(\mathbf{k})$ around the K point, which also induces nodes in the optical absorption in graphite [22].

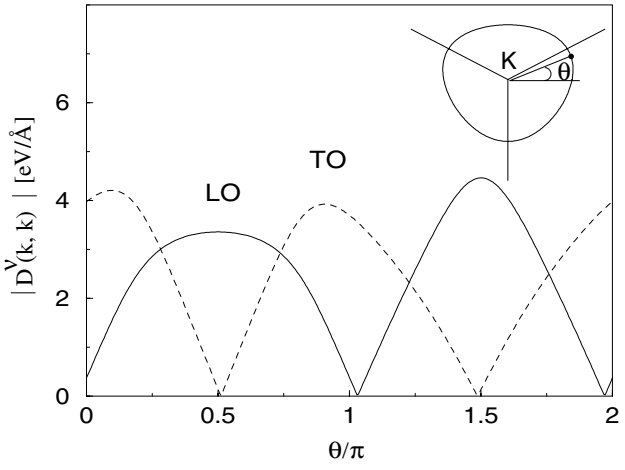

Fig. 2. The $|D^{\nu}(\mathbf{k},\mathbf{k})|$ dependence on $\mathbf{k}$, with $\mathbf{k}$ on an equienergy contour, with energy $E = 1$ eV around a K point (see inset). The two in-plane acoustic modes have zero $D(\mathbf{k},\mathbf{k})$. Solid and dashed lines are for the longitudinal (LO) and tangential (TO) optic modes, respectively. With $\mathbf{k}$ rotation (see the definition of θ in the inset) on the equienergy contour, $|D|$ shows a strong anisotropy.

In Fig. 2 the LO peaks and the TO dips are located at similar θ positions. When we compare Fig. 2 with the Fig. 2 in [22], we find that the e–ph matrix elements $D^{\nu}(\mathbf{k},\mathbf{k})$ for the LO and TO modes have similar oscillating behaviors as the optical matrix elements for the light polarization vectors $\mathbf{P} = (1,0)$ and $(0,1)$, respectively. This interesting finding suggests that by changing the light polarization, we can observe Raman spectra for the LO or TO modes in graphite. The different oscillating behaviors for the LO and TO modes in Fig. 2 also suggest that the ratio of the Raman intensities of the LO and TO modes is dependent on the chiral angle of the carbon nanotubes where special $\mathbf{k}$ points are selected by the so called cutting lines [23,24]. Furthermore, Fig. 2 does not show 3-fold symmetry. The reason is that when the initial state $\mathbf{k}$ rotates along an equienergy contour, then the final state ($\mathbf{k}' = \mathbf{k}$) also rotates along this contour, but $\mathbf{q}$ is fixed to be zero, and thus we cannot expect 3-fold symmetry in $D^{\nu}(\mathbf{k},\mathbf{k})$.

After we obtain the e–ph matrix element $D^{\nu}(\mathbf{k},\mathbf{k}')$, we can calculate the relaxation time by using Eqs. (14)–(16). For a given temperature T, the phonon number can be obtained by Eqs. (8) and (9), and here we take $T = 300$ K, which is the lattice temperature. We show in Fig. 3 the emission and absorption relaxation times (τ_e and τ_a) as a function of energy. For an electron to absorb a phonon, there should exist a phonon in the solid. However, an electron can emit a phonon (+1 in $n^{\nu}(\mathbf{q})$, see Eq. (8)), even though there is no phonon in the solid, since a phonon can be created in this case. Therefore, generally the phonon emission process has more phonons and the electron relaxes faster by phonon emission than by phonon absorption (see Fig. 3). The e–ph relaxation time is determined by the e–ph coupling

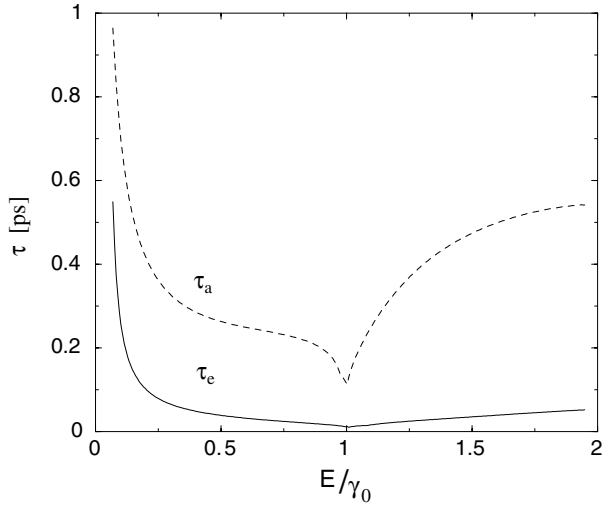

Fig. 3. Electron relaxation time dependence on the initial electron state energy. Solid and dashed lines are for phonon emission τ_e and absorption τ_a, respectively, and the results are for $\gamma_0 = 2.9$ ev and $T = 300$ K.

strength, and by the electron and phonon dispersion relations. The dip in Fig. 3 reflects the van Hove singularity of the electron density of states at the M points in the BZ. When the closed contours for the final electron states approach the equienergy contour connecting the M points, the scattering probability increases due to the large electron density of states and a dip thus appears in Fig. 3. For energy $E \sim 0$, the relaxation time increases dramatically, since the density of final states decreases with decreasing E. This is a special result for graphite, which has only two Fermi points in the 2D BZ. The relaxation time in Fig. 3 is <1 ps, which is comparable with experimental results [3,6]. The experimental data by Hertel and Moos [6] indicate that the e–ph relaxation time in graphite may be in the range of 0.1–0.3 ps in the low energy region.

Fig. 4 gives the inverse of the relaxation time for each of the phonon branches. From Fig. 1 we know that with an increase of the initial state energy, most of the phonon vectors are further away from the Γ (intra-valley case) or the K (inter-valley) points, and thus there are more phonon states that have a large energy. In the energy region of Figs. 3 and 4 ($E > 0.2$ eV), we find that most of the energy–momentum conserved phonon states have an energy larger than $k_B T$. Then, in the phonon emission case, most of the phonons have a similar number $n_{\mathbf{q}}^{\nu} \sim 1$, and thus all branches have the same order of magnitude for the relaxation time, as can be seen from Fig. 4a. As the initial state energy increases, the optical branches in Fig. 4a show some fine structure, which results from the fine structure of the phonon dispersion relations of the optical modes away from the Γ and K points. Around the $E = \gamma_0$ point, there is a sharp peak for each branch due to the large density of states at the M point, since we have more possible final states around the M point to which an electron can be scattered. For the phonon emission process, an electron loses energy by scattering, leading to peak positions for the optical branches that are beyond those for the acoustic branches. The acoustic branch peaks are located close to the $E = \gamma_0$ point due to the smaller phonon energy, and the optical branch peaks away from the $E = \gamma_0$ point due to the larger phonon energy.

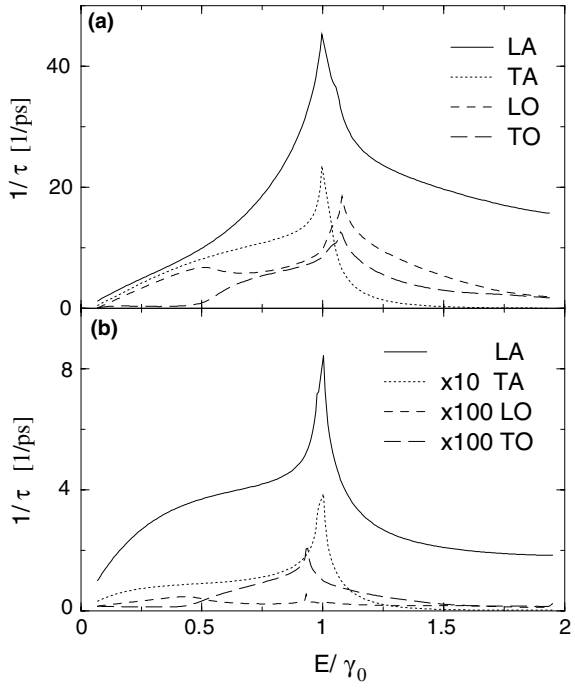

Fig. 4. Inverse of the relaxation time for each phonon branch for (a) phonon emission and (b) phonon absorption. In (b) the values for the optical branches have been amplified by a factor of 100 and the values for the tangential acoustic branches have been amplified by a factor of 10. $\gamma_0 = 2.9$ eV and $T = 300$ K.

In the phonon absorption case, on the other hand, the phonon number is given by Eq. (9), which indicates that the number of optical phonons is very small. The relaxation time for the optical branches is then much smaller compared with that for the acoustic branches, where the phonon can have a small energy. In Fig. 4b the relaxation time for optical phonons has been amplified by 100 times, and their magnitude is still smaller than that for the longitudinal acoustic branches. Between the two acoustic branches, the longitudinal acoustic branch makes a larger contribution to the suppression of the relaxation time due to its larger matrix element [20]. In contrast to the phonon emission process, an electron increases its energy by the absorption of a phonon, and thus the energy where the relaxation time peak positions occur for the optical branches are lower that for the acoustic branches (see Fig. 4b).

By e–e scattering, the photo-excited electrons can reach internal thermalization very quickly. Furthermore, the electrons will relax by e–ph or electron–photon (e–l) scattering. Usually, electrons relax much faster by phonon scattering than by photon scattering, because the relaxation time for phonon scattering is on the order of picoseconds and that by photon scattering is on the order of nanoseconds. For semiconductors there is an energy gap between the conduction and valence bands. When an electron and a hole relax to the bottom of the conduction band and the top of the valence band, respectively, there is no place to which an electron can go and an electron will remain there for some time, after which it will combine with a hole by emitting light. 2D graphite has a special energy band structure. The conduction and valence bands touch each other at the K and K' points. The photo-excited electron therefore goes quickly toward these touching points, since the emission process is faster than the absorption process and the relaxation time is only on the order of 0.1 ps. It thus would seem that the electron will combine with a hole at the touching points without emitting light.

However, a careful check of the relaxation process close to the Fermi surface shows that this is not true. In

Fig. 5 we show the inverse of the emission and absorption relaxation times, $1/\tau_e$ and $1/\tau_a$, for the initial states with energies less than 0.2 eV. Fig. 5 shows that in the higher energy region, the emission relaxation rate $1/\tau_e$ is larger than the absorption relaxation rate $1/\tau_a$, since the emission process has one additional phonon compared to the absorption process. When the initial state energy approaches the Fermi surface, the energy–momentum conserved phonon vectors approach the Γ and K points. The acoustic phonons have a very small energy over the whole closed contours near the Γ point. The main contribution to the relaxation time in the region close to the Fermi surface is by intra-valley acoustic phonon scattering. Because $n^v(\mathbf{q})$ for the intra-valley scattering acoustic phonon process is a large number, the phonon number difference for the emission and absorption processes can be neglected. On the other hand, due to the special electronic structures of graphite, when approaching the Fermi surface the closed contours for the final electron states also shrink quickly and both τ_e and τ_a increase quickly, as can be seen from Fig. 3. The final electron states have a smaller energy in the emission process than in the absorption process. But the energy difference between the two processes is small for the intra-valley acoustic phonon scattering, when the phonon energy is small. Thus, the closed contour for the final electron states shrinks a bit more quickly in the emission process, and consequently τ_e increases a bit more quickly than τ_a. Therefore, when the initial state moves toward the Fermi surface, one expects a point to occur where $\tau_e = \tau_a$. For electron energies greater than this point E_{point}, $\tau_e < \tau_a$, but for electron energies lower than E_{point} τ_e remains approximately equals to τ_a for a distance and then exceeds τ_a slightly. In Fig. 5 the position for this point is $E = 0.11$ eV. Clearly, above an electron energy of $E = 0.11$ eV, the difference between τ_e and τ_a is obvious, while below $E = 0.11$ eV the difference between τ_e and τ_a becomes small.

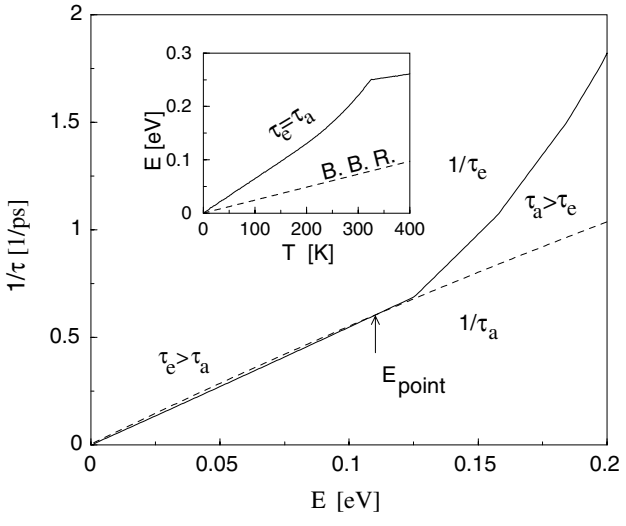

Fig. 5. Inverse of the relaxation time in the low electron energy region for emission and absorption. Solid and dashed lines are for emission and absorption, respectively. A crossing point for these two lines is obtained. The inset shows the energy position for $\tau_e = \tau_a$ as a function of temperature. The dashed line of the inset denotes the peak positions of the intensity for Planck's black-body radiation (BBR).

The electron energy E_{point} where $\tau_e = \tau_a$ has important implications. If the laser energy $E_{laser} > 2E_{point}$, the photo-excited electron goes quickly toward this point. After the electron reaches E_{point}, phonon emission and absorption reach dynamic equilibrium and the number of electrons becomes stable at this energy. This special point may provide a platform for an electron to remain at the same energy for a long time, since the probabilities for an electron to absorb and emit a phonon are the same. Thus, E_{point} functions similar to the bottom of the conduction band in a semiconductor. Light emission is then expected around this point. In contrast, if $E_{laser} < 2E_{point}$, the photo-excited electron reaches quasi-equilibrium for phonon emission and absorption, and it favors moving a bit upward in energy before emitting light. This property suggests to us to consider graphite as a black-body. In the inset of Fig. 5, we plot the dependence of $2E_{point}$ on temperature. The photon energy ($h\nu_{max}$) at the peak of the general (not 2D) black-body radiation (BBR) intensity at different temperatures is also shown. A perfect black-body should show strict equilibrium for photon emission and absorption around $h\nu_{max}$. From the inset of Fig. 5 we can see that $h\nu_{max}$ is always below $2E_{point}$ and is in the region where $\tau_e \approx \tau_a$. For example at $T = 300$ K, $2E_{point} = 0.22$ eV and $h\nu_{max} = 0.072$ eV. For the conduction band, an electron with energy $E = h\nu_{max}/2$ has $\tau_e = 5.2$ ps and $\tau_a = 4.9$ ps. This means that graphite has a similar absorption and emission photon frequency which is around $h\nu_{max}$. Therefore, graphite is considered to be a good black-body material.

4. Summary

In summary, we have studied electron relaxation in graphite in terms of the e–ph interaction process. The obtained e–ph matrix elements for the Γ point phonon modes show strong anisotropy around the K point, which indicates that the ratio of the G band Raman intensities of the LO and TO modes is dependent on the chiral angle of the carbon nanotubes. We have calculated the relaxation time over a wide energy region. We find that generally all modes make the same order of magnitude contribution in the phonon *emission* process, but only the *longitudinal* acoustic modes make a dominant contribution in the phonon *absorption* process. However, in the energy region close to the Fermi level, the dominant contribution is from longitudinal acoustic modes for both emission and absorption. In the low electron energy region, where we consider a microscopic view of BBR, we find a quasi-stable point for the

emission and absorption rates, which has interesting implications for the e–ph interaction in this region.

Acknowledgements

R.S. acknowledges a Grant-in-Aid (No. 13440091) from the Ministry of Education, Japan. MIT authors acknowledge support under NSF Grants DR 01-16042, and INT 00-00408.

References

[1] P.M. Echenique et al., Chem. Phys. 251 (2002) 1.
[2] H. Petek, S. Ogawa, Prog. Surf. Sci. 56 (1997) 239.
[3] K. Seibert, G.C. Cho, H. Kurz, W. Kutt, D.H. Reitze, J.I. Dadap, H. Ahn, M.C. Downer, Phys. Rev. B 42 (1990) 2842.
[4] T. Hertel, G. Moos, Phys. Rev. Lett. 84 (2000) 5002.
[5] O.J. Korovyanko, Z.V. Vardeny, C.X. Sheng, A.B. Dalton, R.H. Baughman, Phys. Rev. Lett. 92 (2004) 017403.
[6] T. Hertel, G. Moos, Chem. Phys. Lett. 320 (2000) 359.
[7] G. Moos, R. Fasel, T. Hertel, J. Nanosci. Nanotechnol. 3 (2003) 145.
[8] J.E. Fischer, H. Dai, A. Thess, N.M. Hanjani, D.L. Dehaas, R.E. Smalley, Phys. Rev. B 55 (1997) R4921.
[9] L.X. Benedict, V.H. Crespi, S.G. Louie, M.L. Cohen, Phys. Rev. B 52 (1995) 14935.
[10] Z.M. Li, Z.K. Tang, H.J. Liu, N. Wang, C.T. Chan, R. Saito, S. Okada, G.D. Li, J.S. Chen, N. Nagasawa, S. Tsuda, Phys. Rev. Lett. 87 (2001) 127401.
[11] M.J. O'Connell, S.M. Bachilo, X.B. Huffman, V.C. Moore, M.S. Strano, E.H. Haroz, K.L. Rialon, P.J. Boul, W.H. Noon, C. Kittrell, J. Ma, R.H. Hauge, R.B. Weisman, R.E. Smalley, Science 297 (2002) 593.
[12] R.B. Weisman, S.M. Bachilo, Nanoletters 3 (2003) 1235.
[13] J. Lefebvre, Y. Homma, P. Finnie, Phys. Rev. Lett. 90 (2003) 217401.
[14] Y. Miyauchi, S. Chiashi, Y. Murakami, Y. Hayashida, S. Maruyama, Chem. Phys. Lett. 387 (2004) 198.
[15] R. Saito, A. Grüneis, Ge.G. Samsonidze, V.W. Brar, G. Dresselhaus, M.S. Dresselhaus, A. Jorio, L.G. Cançado, C. Fantini, M.A. Pimenta, A.G. Souza Filho, New J. Phys. 5 (2003) 157.1.
[16] A. Jorio, R. Saito, M.S. Dresselhaus, G. Dresselhaus, dhfksa dafda, in: Andrea Ferrari, John Robertson (Eds.), Philosophical Transactions of the Royal Society: Special Issue, Raman spectroscopy in carbons: from nanotubes to diamond, Royal Society, Oxford UK, 2004.
[17] S. Xu et al., Phys. Rev. Lett. 76 (1996) 483.
[18] G. Moos, C. Gahl, R. Fasel, M. Wolf, T. Hertel, Phys. Rev. Lett. 87 (2001) 267402.
[19] R. Saito, G. Dresselhaus, M.S. Dresselhaus, Physical Properties of Carbon Nanotubes, Imperial College Press, London, 1998.
[20] L. Pietronero, S. Strässler, H.R. Zeller, M.J. Rice, Phys. Rev. B22 (1980) 904.
[21] R.A. Jishi, M.S. Dresselhaus, G. Dresselhaus, Phys. Rev. B 48 (1993) 11385.
[22] A. Grüneis, R. Saito, Ge.G. Samsonidze, T. Kimura, M.A. Pimenta, A. Jorio, A.G. Souza Filho, G. Dresselhaus, M.S. Dresselhaus, Phys. Rev. B 67 (2003) 165402.
[23] R. Saito, T. Takeya, T. Kimura, G. Dresselhaus, M.S. Dresselhaus, Phys. Rev. B 57 (1998) 4145.
[24] Ge.G. Samsonidze, R. Saito, A. Jorio, M.A. Pimenta, A.G. Souza Filho, A. Grüneis, G. Dresselhaus, M.S. Dresselhaus, J. Nanosci. Nanotechnol. 3 (2003) 431.